Journal of Marine Science and Technology

Volume 20 | Issue 5 Article 14

INVERTING SEDIMENT SOUND SPEED PROFILE USING A PARAMETERIZED GEOACOUSTIC MODEL: NUMERICAL AND STATISTICAL ANALYSIS

Chen-Fen Huang
Institute of Oceanography, National Taiwan University, Taipei, Taiwan, R.O.C.

Shih-Feng Yang
Institute of Applied Marine Physics and Undersea Technology, National Sun Yat-sen University, Kaohsiung, Taiwan, R.O.C.

Jin-Yuan Liu
Institute of Applied Marine Physics and Undersea Technology, National Sun Yat-sen University, Kaohsiung, Taiwan, R.O.C. National Taitung University, Taitung, Taiwan, R.O.C., jimliu@faculty.nsysu.edu.tw

Recommended Citation

Huang, Chen-Fen; Yang, Shih-Feng; and Liu, Jin-Yuan (2012) "INVERTING SEDIMENT SOUND SPEED PROFILE USING A PARAMETERIZED GEOACOUSTIC MODEL: NUMERICAL AND STATISTICAL ANALYSIS," *Journal of Marine Science and Technology*: Vol. 20: Iss. 5, Article 14.
DOI: 10.6119/JMST-012-0712-1
Available at: https://jmstt.ntou.edu.tw/journal/vol20/iss5/14

INVERTING SEDIMENT SOUND SPEED PROFILE USING A PARAMETERIZED GEOACOUSTIC MODEL: NUMERICAL AND STATISTICAL ANALYSIS

Acknowledgements

This work was supported in part by National Science Council of Taiwan, R.O.C. through contract NSC 98-2611-M-002- 017-MY3, NSC 99-2221-E-110-093, and by the Ministry of Education of Taiwan, R.O.C. under the project entitled Aim for Top University-Asian Pacific Ocean Research Center (95C100303). The authors would like to express our profound thanks for their financial support.

Journal of Marine Science and Technology, Vol. 20, No. 5, pp. 584-594 (2012)
DOI: 10.6119/JMST-012-0712-1

INVERTING SEDIMENT SOUND SPEED PROFILE USING A PARAMETERIZED GEOACOUSTIC MODEL: NUMERICAL AND STATISTICAL ANALYSIS

Chen-Fen Huang[1], Shih-Feng Yang[2], and Jin-Yuan Liu[2,3]

Key words: geoacoustic inversion, generalized-exponential and inverse-square functions, parameter sensitivity analysis, uncertainty analysis, statistical estimation of inverted sound speed.

ABSTRACT

The objective of this paper is to develop and evaluate an inversion algorithm for estimating the parameters in a geoacoustic model for a marine sediment layer. The geoacoustic model employs a generalized-exponential function for sound speed profile, and an inverse-square function for density distribution. Based upon plane-wave reflection from a non-uniform sediment layer overlying an elastic seafloor, an inversion procedure is established and numerically implemented for estimating the parameters using synthetic noise-contaminated data. The sensitivity of each model parameter is first studied, and then three highly sensitive parameters in the geoacoustic model and one statistical parameter are chosen for inversion analysis. The resulting sound speed profiles from the inversion are analyzed by a probabilistic approach, which is quantified by the posterior probability density for the uncertainties of the estimated parameters. The parameter uncertainties referenced to 1-D and 2-D marginal posterior probability densities are investigated, followed by the statistical estimation for the sound speed profile in terms of a 95% credibility interval. We demonstrate the effects of, the signal-to-noise ratio (SNR), the dimension of the data vector, and the region in which the data are sampled, on the statistical estimation of the sound speed profile, and offer physical interpretations about the statistical variations attributable to these effects. This analysis provides a basis for estimating the acoustic properties of a continuously-stratified layer using inversion approach, and is particularly useful for a medium with properties describable by analytical functions.

Paper submitted 11/07/11; revised 06/19/12; accepted 07/12/12. Author for correspondence: Jin-Yuan Liu (e-mail: jimliu@faculty.nsysu.edu.tw).

[1] *Institute of Oceanography, National Taiwan University, Taipei, Taiwan, R.O.C.*
[2] *Institute of Applied Marine Physics and Undersea Technology, National Sun Yat-sen University, Kaohsiung, Taiwan, R.O.C.*
[3] *National Taitung University, Taitung, Taiwan, R.O.C.*

I. INTRODUCTION

Geoacoustic inversion using active or passive acoustic processes for the estimation of the geoacoustic properties, such as density and sound speed of the seabed, has been an interest of research in the underwater acoustics community in the past two decades [1, 6, 14, 23, 25], in particular, many works using reflection measurements received on either a vertical or horizontal array [3, 4, 10-12]. The approach is particularly valuable for estimating the parameters that are difficult to measure directly on site, e.g., the thickness, layering structure, and shear sound speed of the sediment. Recent advancements on signal processing techniques and numerical algorithms for geoacoustic inversion, such as SAGA [7], have demonstrated that inversion is an effective approach for evaluating marine environmental parameters, despite the fact that the estimation uncertainties caused either by noise and/or modeling variations are still of many concerns [5, 13, 16].

In performing geoacoustic inversion, it is required to establish a prior parameterized seismo-acoustic environmental model, in which the parameters to be estimated are embedded. For the seabed, the general practice is to assume that the sediment layer is consisted of one or several uniform layers, each possessing a constant value of density and sound speed. However, many geoacoustic surveys have shown that the seabed properties may vary continuously, and in some cases, may be described by a parameterized model [8, 9]. In this study, we shall assume that the density profile $\rho(z)$ and sound speed distribution $c(z)$ of the sediment layer may be, respectively, represented by a generalized-exponential function and an inverse-square function as shown below [21]:

$$\rho(z) = \frac{Ae^{\beta z}}{(e^{\beta z} + a)^2}, \tag{1}$$

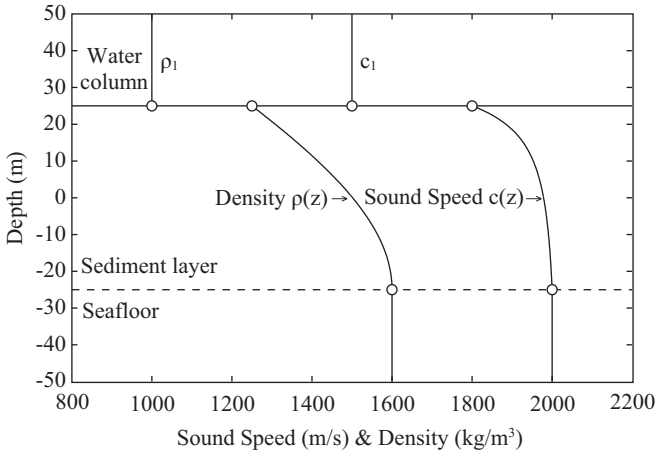

Fig. 1. A representative density and sound speed profiles corresponding to Eqs. (1) and (2), with the following value of parameters: β = 0.020285, a = 0.60222, A = 3854.2118, b = 0.745, γ = 0.024959, $c_{2\text{mid}}$ = 1978.6 m/s.

$$c(z)=\frac{1}{\left[\dfrac{b^2}{c_1^2}+\left(\dfrac{1}{c_{2\text{mid}}^2}-\dfrac{b^2}{c_1^2}\right)\dfrac{1}{(1-\gamma z)^2}\right]^{1/2}}, \qquad (2)$$

where A, β, a, c_1, b, $c_{2\text{mid}}$, and γ are constant parameters relating to the variation of the profiles, in particular, $c_{2\text{mid}}$ is the sound speed at the middle of the sediment layer; a set of representative profiles described by the model is shown in Fig. 1. Here, we would like to stress that the reason for adopting this model is not only because it is capable of describing a continuously-stratified seabed environment, but also because it renders an analytical solution for the acoustic wave equation [21], making the model particularly useful in practical applications and numerical simulations.

The objective of this paper is to establish the procedure for estimating the model parameters and quantifying their uncertainties using geoacoustic inversion and statistical analysis. It is noted that the inversion of the model parameters represents the profile of the complete non-uniform layer, which would otherwise be required to be divided into many sub-layers, leading an inversion with high dimensionality a very time-consuming or even an unstable process. Bearing this advantage, however, we do not intend to claim that the geoacoustic model considered here may be applied universally, rather, their applications may only be restricted to the cases where the variations and assumptions invoked have suited the formulation in a realistic situation.

In the following sections, the forward problem of a plane-wave reflection from a non-uniform seabed is first established and formulated. Then, the theory of inversion employing a probabilistic approach is described. The sensitivity of each of the model parameters is analyzed based upon the solutions of the forward problem, leading to the choice of four highly sensitive parameters to be estimated by inversion. The analysis for the inversion quality represented by the credibility interval is carried out by the numerically-generated results with respect to the effects of SNR, the number of data set, and the sampling region of the grazing angles.

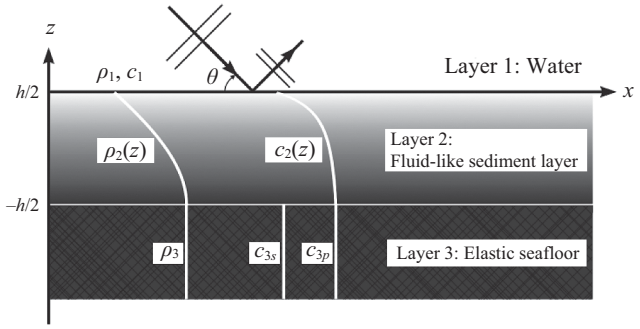

Fig. 2. A schematic diagram for plane-wave reflection from a non-uniform sediment layer overlying an elastic seafloor.

II. THE FORWARD PROBLEM: PLANE-WAVE REFLECTION FROM A NON-UNIFORM SEABED

The present analysis is based on the problem of plane-wave reflection from a non-uniform fluid-like sediment layer overlying an elastic seafloor, as schematically shown in Fig. 2. The density and compressional sound speed of the sediment layer are assumed to behave as Eqs. (1) and (2), respectively, and the seafloor (or sea basement) includes a shear sound speed to account for elasticity of the medium.

The mathematical formulation for solving the reflection problem is rather straightforward, and is similar to those presented in the previous studies by the authors [17, 18]. Here, for completeness, the derivation and formulation are briefly summarized in Appendix A. It is noted that the solutions of the acoustic wave equation for the non-uniform sediment layer, derived by Robins [21], involve the Hankel functions, as shown in Eqs. (A5) - (A10), which, for high frequencies, may involve imaginary orders (see Eq. (A9)). While evaluation of the Hankel function presents no difficulty for real orders in modern computational software, such as MATLAB; however, for imaginary orders, it requires special treatments for its stability during evaluation.

In this study, the inversion is based upon synthetic noise-contaminated data that simulate the measured reflection coefficients. Here, the problem of plane-wave reflection from a non-uniform seabed, referred to as the forward problem, provides the reflection coefficient for constructing the objective function and the seismo-acoustic seabed as the environmental model; both are required when producing the replica in the inversion process. The main effort is then to estimate the parameters that are imbedded in the sound speed and/or density profiles of the sediment layer.

III. THE INVERSION THEORY: PROBABILISTIC APPROACH

In a probabilistic approach, the solution to determining the parameters of interest **m**, given an observed data **d**, is characterized by the posterior probability density (PPD) $p(\mathbf{m}|\mathbf{d})$. First, the prior information about the model parameter vector is quantified by the probability density function (pdf) $p(\mathbf{m})$. Then, this information is combined with the likelihood function $p(\mathbf{d}|\mathbf{m})$ provided by the combination of data and the physical model to give the posterior information of the model parameters $p(\mathbf{m}|\mathbf{d})$. A complete discussion of inverse theory from a probabilistic point of view may be found in the textbook by Tarantola [24]. Additional details of Monte Carlo sampling of posterior distributions can be found in the paper by Mosegaard and Sambridge [20].

According to Bayes' theorem the solution to the inverse problem can be expressed as:

$$p(\mathbf{m}|\mathbf{d}) = \frac{p(\mathbf{d}|\mathbf{m})p(\mathbf{m})}{p(\mathbf{d})} \propto L(\mathbf{m})p(\mathbf{m}), \tag{3}$$

where $p(\mathbf{d})$ is a normalizing factor that makes the integral of the posterior pdf equal to unity; since it does not depend on environmental model **m**, it is typically ignored in parameter estimation, and then $L(\mathbf{m})$ is used to denote the likelihood function $p(\mathbf{d}|\mathbf{m})$. The posterior distribution $p(\mathbf{m}|\mathbf{d})$ carries all information available on models originating from the data and from data-independent prior information.

The posterior probability density provides the full description of the state of knowledge about model parameters after observing the data. To interpret the multidimensional PPD, marginalization is used to summarize the PPD for a single parameter m_i by integrating over the remaining parameters $\mathbf{m}'$ to give:

$$p(m_i|\mathbf{d}) = \int p(m_i, \mathbf{m}'|\mathbf{d})\,d\mathbf{m}'. \tag{4}$$

Also, the 2-D marginal probability distributions of paired parameters can be obtained in a similar way. It is often desirable to characterize the distribution in terms of its most probable value of the posterior, also known as the maximum *a posteriori* (MAP) estimate:

$$\mathbf{m}_{\text{map}} = \arg\max_{\mathbf{m}} p(\mathbf{m}|\mathbf{d}), \tag{5}$$

where $\arg\max_{\mathbf{m}}$ stands for the argument of the maximum over the parameter space of **m**.

1. The Likelihood Function

Let **d** denote the observed data vector, which in the present context contains the measured reflection coefficients for a total number of N grazing angles sampled. Also, let $\mathbf{G}(\mathbf{m})$ represent the predicted data vector based upon a parameterized environmental model for a given parameter vector **m**. Then, the measurement noise vector **n**, defined as the difference between the observed data **d** and the predicted data $\mathbf{G}(\mathbf{m})$, is given as:

$$\mathbf{n} = \mathbf{d} - \mathbf{G}(\mathbf{m}). \tag{6}$$

Assuming that the measurement noises may be described by independent and identically distributed (iid) Gaussian with zero mean and common error variance ν over the selected grazing angles, then the likelihood function can be expressed as:

$$L(\mathbf{m}) = p(\mathbf{d}|\mathbf{m}) = \frac{1}{(2\pi\nu)^{N/2}} \exp\left(-\frac{\mathbf{n}^T\mathbf{n}}{2\nu}\right), \tag{7}$$

where the superscript T denotes the transpose. It is seen that the probability of having observed the data **d** is reduced as the sum of squared error increases, implying that the likelihood function quantifies the information about **m** contained in the data.

In many cases, the data error variance v is not known, but can be estimated by including it in the model parameter vector as one of the parameters to be inverted [13], therefore, the likelihood function can be expressed as:

$$L(\mathbf{m}, \sigma_1, \ldots, \sigma_N) \propto \exp\left(-\sum_{j=1}^{N} \frac{[d_j - G_j(\mathbf{m})]^2}{2\sigma_j^2} - \ln\prod_{j=1}^{N}\sigma_j\right), \tag{8}$$

where d_j is the observed value at the jth grazing angle and $G_j(\mathbf{m})$ is the replica generated for the parameter vector **m** at the same grazing angle.

We shall carry out the geoacoustic inversion using synthetic noise-contaminated data to simulate the measured reflection coefficients **d**, which can be represented as:

$$\mathbf{d} = \mathbf{G}(\mathbf{m}_{\text{true}}) + \mathbf{n}, \tag{9}$$

where $\mathbf{m}_{\text{true}}$ is the vector containing the true value of the parameter, and **n** is the random noise vector with its components being an iid Gaussian and zero-mean distribution with a designated signal to noise ratio (SNR).

For a given value of SNR, the standard deviation of the jth component of the measured data can be expressed as:

$$\sigma_j = G_j(\mathbf{m}_{\text{true}})10^{-\text{SNR}/20}, \tag{10}$$

which shows that the error standard deviation is proportional to the magnitude of the measured data. Therefore, from Eq. (8), the likelihood function can be written as:

$$L(\mathbf{m}, \nu) \propto \exp\left(-\frac{1}{2\nu}\phi(\mathbf{m}) - \frac{N}{2}\ln\nu\right), \tag{11}$$

where ν denotes the normalized error variance given by $\nu = (\sigma_j/d_j)^2$, and $\phi(\mathbf{m})$ is the objective function, measuring the misfit between the measured and modeled data, defined as:

$$\phi(\mathbf{m}) = \sum_{j=1}^{N} \frac{\left[d_j - G_j(\mathbf{m})\right]^2}{d_j^2}. \tag{12}$$

The resulted objective function weights all data equally, since the contribution of each reflection coefficient to the total misfit is normalized by its received signal strength. In other words, this objective function regards the measured reflection coefficients from different angles (paths) as equally important. However, if the objective is to seek a best-fit geoacoustic model, one could weight the reflection data for each angle proportionally to its strength, so that it yields an optimum model that may account for variation of attenuation from various angles.

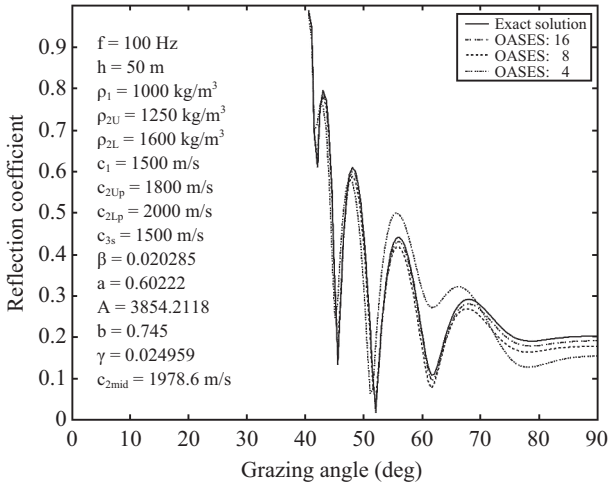

Fig. 3. Comparison of the reflection coefficient from the analytic formula from present study with those using OASES for increasing number of subdivision.

2. Probability Distribution of Sound Speed Profile

In this analysis, the inversion of sound speed profile $c(z)$ and its associated uncertainty are the major subject of interests. Based upon the posterior distribution $p(\mathbf{m}\,|\,\mathbf{d})$ for the estimated parameters $\mathbf{m}$, the posterior distribution $p(\mathbf{c}\,|\,\mathbf{d})$ for the sound speed profile $\mathbf{c}$ may be obtained, and then all other relevant statistics follow. Here, we use $\mathbf{c}$ to denote the vector containing sound speed components at various depths, i.e., $c_i = c(z_i)$.

For either the prior or posterior probability distribution of the sound speed profile, the probability distribution of $\mathbf{c}$ may be expressed as:

$$p(\mathbf{c}\,|\,\mathbf{d}) = \int_M \delta[\mathbf{C}(\mathbf{m}) - \mathbf{c}]\, p(\mathbf{m}\,|\,\mathbf{d})\, d\mathbf{m} \tag{13}$$

where M represents the model domain and $\delta[\mathbf{C}(\mathbf{m}) - \mathbf{c}]$ is equivalent to $\mathbf{c} = \mathbf{C}(\mathbf{m})$, which reconstructs the sound speed profile for each value of $\mathbf{m}$, in reference to the formula given by Eq. (2).

As for the characterization of the statistics, since the full probability distributions of the sound speed are available and they are not Gaussian, it is preferable to characterize the distributions with the medians and the intervals that contain 95% of the highest probability density, referred to as the Credibility Interval (CI) in Bayesian terminology, rather than using the means and standard deviations for Gaussian distributions [2].

IV. SOLUTIONS OF FORWARD PROBLEM AND SENSITIVITY ANALYSIS

Before carrying out the inversion analysis, we need to solve the forward problem, and ensure the correctness of the solutions. Furthermore, each of the parameters in the geoacoustic model is examined with respect to its impact on the solution so that its *sensitivity* on the output is assessed. Only those parameters that associate with high sensitivity shall be chosen for inversion.

1. Solutions of the Forward Problem

The linear system, Eq. (A20), for solving the forward problem derived in Appendix A, can be solved numerically to obtain the reflection coefficient, A_1^+ in Eq. (A11). It is worth mentioning that, although the solution procedure is straightforward, the functions G and H in Eq. (A5) and their derivatives in the coefficient matrix $\tilde{B}$, Eq. (A21), require special treatments, because numerical evaluation of these functions may incur instability issues if the orders of Hankel functions become imaginary; relevant discussion has been given in the previous work by the authors [19].

To ensure the correctness of the numerical algorithms, a canonical set of parameters is supplied to generate the numerical solution. The solution is then compared with the asymptotic results obtained from existing software OASES [22], which is generally accepted as one of the most efficient computational software for solving seismic acoustic wave propagation in a horizontally-stratified medium. Fig. 3 illustrates the reflection coefficients for frequency of 100 Hz and for the set of parameters shown in the figure. It is seen that the results computed from OASES, with increasing number of discrete layers from 4 to 16, consistently approach to the exact solution obtained from present analysis, ensuring the reliability of the numerical algorithms for the solution of the forward problem employed in the present study.

2. Sensitivity Analysis

It is well understood that inversion for the environment parameters is a highly nonlinear process, and frequently subjects to non-uniqueness problem. Therefore, a prior knowledge either on the environmental model itself or the effect of model parameter variation on the outputs, referred to parameter

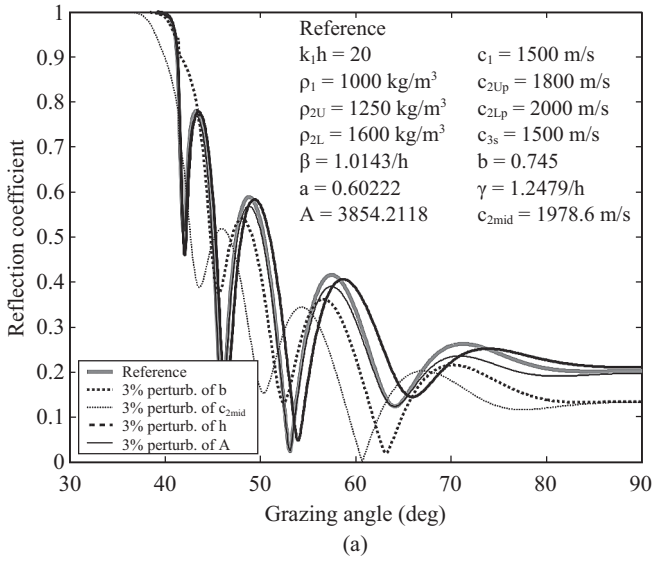

Fig. 4. Reflection coefficients for various parameters with 3% perturbation for frequency 100 Hz.

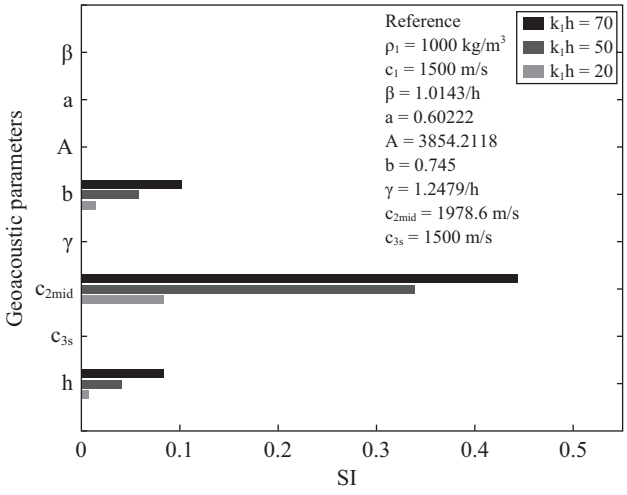

Fig. 5. The sensitivity index (SI) for the model parameters.

sensitivity, provides important information for choosing the parameters to be inverted. To serve this purpose, we examine the deviation or mismatch of the reflection coefficient due to the variation of various parameters.

Fig. 4 demonstrates the effects various model parameters on the reflection coefficients. Here, a nominal value for each parameter shown in the figure is chosen to derive a solution as a benchmark, and then a deviation of 3% of parameters values is *individually* perturbed to obtain its corresponding results. These results reveals that the variations of the parameters b, $c_{2\text{mid}}$, and h result in much more significant deviations than those due to others, indicating that these three parameters, all related to the sound speed profile, have much higher local impact on the overall results, and therefore, have a higher sensitivity.

For quantitative analysis, an index gauging parameter sensitivity, referred to as sensitivity index SI(m_i) for parameter m_i, is defined as follows:

$$\text{SI}(m_i) = \frac{1}{N}\sum_{j=1}^{N}\frac{[G_j(m_i) - G_j(\mathbf{m}_{\text{ref}})]^2}{G_j^2(\mathbf{m}_{\text{ref}})} \tag{14}$$

where N is the total number of grazing angles sampled, and $G_j(\mathbf{m}_{\text{ref}})$, $G_j(m_i)$ are the magnitudes of reflection coefficients at the jth angle for reference model $\mathbf{m}_{\text{ref}}$ and for the parameter m_i, respectively. Fig. 5 shows the SI of all parameters relating to sediment layer for three values of frequency represented by k_1h. It is seen that the parameters b, $c_{2\text{mid}}$, and h have much higher SI than any other parameters, particularly for higher values of k_1h.

Although, in theory we may invert all parameters, however, in view of the analysis of SI's of various parameters, we shall concentrate on the inversion of the sound speed profile of the sediment layer in correspondence to the three higher sensitive parameters. In addition, the data error variance ν, as shown in Eq. (7), is also included as one of the parameters to be estimated during the inversion.

V. RESULTS AND DISCUSSION

Since the purpose of this study is to demonstrate the inversion algorithm for environmental model parameters, the employed model data are synthesized through numerical simulation. Here, an environmental model with a nominal set of parameters is chosen to generate the reflection coefficients as the modeled data $\mathbf{G}(\mathbf{m})$, then a certain amount of random noise $\mathbf{n}$ parameterized by SNR is superimposed to yield the noise-contaminated data, which is treated as the field measurements for the inversion analysis in this study.

The algorithm described in Sec. III is now numerically implemented for the inversion of sound speed profile. Since

the computational expenses are of little concern for an inversion with only four parameters, an exhaustive evaluation of $p(\mathbf{m}\,|\,\mathbf{d})$ over a grid of parameter space combined with ordinary numerical integration is executed. The exhaustive search is a robust and accurate approach and is recommended for inversion with only a few parameters (e.g., less than eight). However, if the number of parameters is large, Monte Carlo methods of numerical integration should be used.

For the present analysis, the parameter vector **m** denotes $\mathbf{m} = (b, c_{2\text{mid}}, h)$, and the data vector **d** contains the *randomized* reflection coefficients at selected grazing angles as its components. The parameter intervals within which a reasonable sound speed profile may be generated are chosen to be as follows: $0.735 \le b \le 0.749$, $1960 \le c_{2\text{mid}} \le 2010$, and $90 \le h \le 110$; these are the intervals in which the parameters are searched to generate the best likelihood of the estimation.

1. Analysis of Parameter Uncertainty

The baseline environment consists of a 100-m non-uniform sediment layer overlying on a semi-infinite elastic basement; the true values for the related parameters are given in Fig. 6(a); these values are merely chosen for illustrative purpose. In the figure, the dashed line represents the original noise-free reflection coefficients from the baseline model for frequency 200 Hz. The reflection coefficients are measured at four grazing angles: 75°, 80°, 85°, and 90°. To simulate a set of noise-contaminated data, we add to the modeled reflection field **G(m)** a noise vector consisting of elements drawn from a computer-generated approximation to zero-mean uncorrelated Gaussian random numbers with 20-dB SNR (equivalent to $\nu = 0.01$); the observed data are shown as the circles with error bars in Fig. 6(a).

Fig. 6(b) shows the parameter uncertainty computed from the simulated data for the above-chosen geoacoustic parameters and the error variance ν. Since the parameter vector **m** is of dimension four, it is difficult to visualize it in a hyperspace geometry, therefore, the marginal probabilities described in Eq. (4) are used to summarize the structure of the PPD. The line subplots along the diagonal are the one-dimensional (1-D) marginal PPDs for each parameter, $p(m_i\,|\,\mathbf{d})$, and the contour subplots in the upper triangle are the 2-D marginal PPDs corresponding to the paired parameters in the bottom-most and left-most line subplots, $p(m_b, m_i\,|\,\mathbf{d})$. Gray levels represent the probability density. Darker shades mean higher probability density of observing the estimated parameter value given the data. The 1-D and 2-D marginal PPDs reveal the uncertainty of the parameter estimation, in addition, the 2-D PPDs also show the correlations between the paired parameters. For example, the contour subplot on row 1 and column 1 shows the correlation between $c_{2\text{mid}}$ and b. The result suggests that there is a strong negative coupling between these two parameters. Therefore, the inter-parameter correlation results in a relatively flat distribution in the 1-D marginal PPDs for the parameters $c_{2\text{mid}}$ and b. If more information about one of these two parameters could be obtained, then the 1-D marginal PPD of the other parameter could be sharpened.

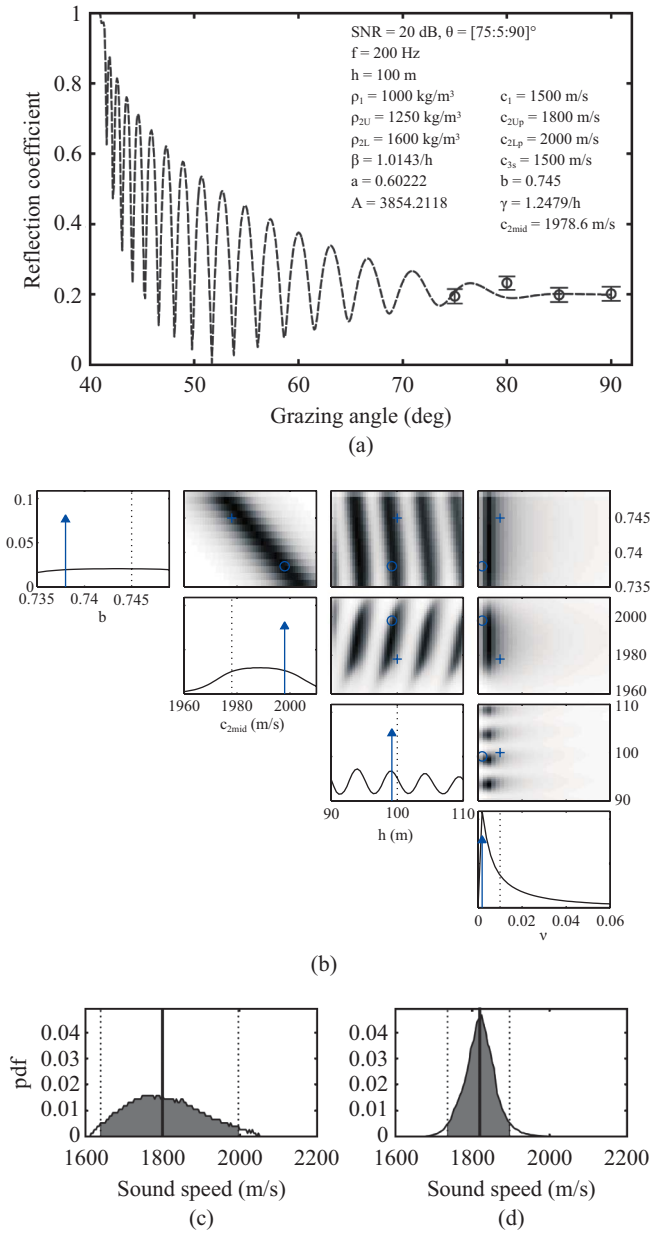

Fig. 6. Uncertainty analysis for the measured reflection coefficients at 75°, 80°, 85° and 90° for SNR = 20 dB. (a) data with uncorrelated Gaussian noise. The circles are the noise-contaminated data with error bars at ±1σ; the dashed line indicates the original noise-free reflection coefficient. (b) 1-D and 2-D marginal posterior probability densities (PPDs) for the geoacoustic parameters as well as the error variance. The arrow and circle indicate the estimated optimum value for the model parameter; while vertical dotted line and plus sign indicate the true value. (c) marginal prior and (d) marginal posterior probability distributions of the reconstructed sediment sound speed at 0-m depth.

Due to the nature of the reflection coefficients, the PPDs may be sensitive to the parameters chosen. For example, the uncertainty of h exhibits a multimodal structure: several

maxima of magnitude in p(h|**d**) and multiple valleys in the 2-D joint PPDs paired with the sediment thickness h. In general, it is difficult to summarize its posterior with a few numbers, therefore, the p(**m**|**d**) is used to reconstruct the sediment sound speed profile.

Figs. 6(c) and (d) show the probability distributions for the sediment sound speed at 0-m depth, i.e., the upper interface of the sediment layer. Panel (c) shows the prior probability distribution of the surficial sound speed using data-independent prior information, while (d) shows the posterior probability distribution of the sound speed using all information available on models embedded in the data and from data-independent prior information. Since more information is provided to reconstruct the sound speed, the posterior uncertainty of surficial sediment sound speed is reduced. Often, the distribution of the sediment sound speed is poorly approximated by a Gaussian distribution, the central tendency and spread of the sound speed distribution are indicated, respectively, by the median (the heavy vertical line) and the 95% Credibility Interval (CI; the gray area), which means that the probability of sound speed lying in this interval is at least 95% [2].

2. Statistical Estimation of Sediment Sound Speed Profiles

The reconstructed sound speed profiles based upon the synthetic randomized data using inversion algorithms are presented and discussed in this section. Since the inversion is subject to statistical variation due to addition of noise, the 95% CIs estimation of the sound speed profiles as addressed in the previous section is our primary interest. Also, we shall examine the effects of SNR, dimension of data vector, and sampling range of the measurement on the quality of estimation.

Fig. 7 shows the CIs of the reconstructed sediment sound speed profile using the reflection coefficients measured at 75°, 80°, 85°, and 90°, for the prior case (a), and for the posterior cases with SNR equal to 10 dB (b), 20 dB (c), and 30 dB (d), respectively. For convenience in presentation to correspond to the physical situation, the origin is set at the top of the layer, and vertical axis z points downward and is normalized as k_1z. It is first noted that the dashed curve represents the true sound speed profile as the benchmark solution, and the solid curve shows the median of the statistical distribution, which is taken to be the *nominal* sound speed profile from the inversion. It should be stressed that although the median (or other statistics such as mean) may be considered as an estimate of the inversion of the sound speed, the statistical estimation of the sound speed profiles represented by 95% CI bears more significance in showing the inversion quality than the median itself, because it sheds light on the overall behavior of the inverted sound speed profile in terms of qualitative nature.

The results in Fig. 7 demonstrate that the uncertainties for the prior case are much larger than those corresponding to the posterior cases, and furthermore, the uncertainties are reduced in accordance with the increase of SNR, with SNR = 30 dB giving estimation rather close to real values. This is clear in that, for the prior case, the results are based upon knowledge

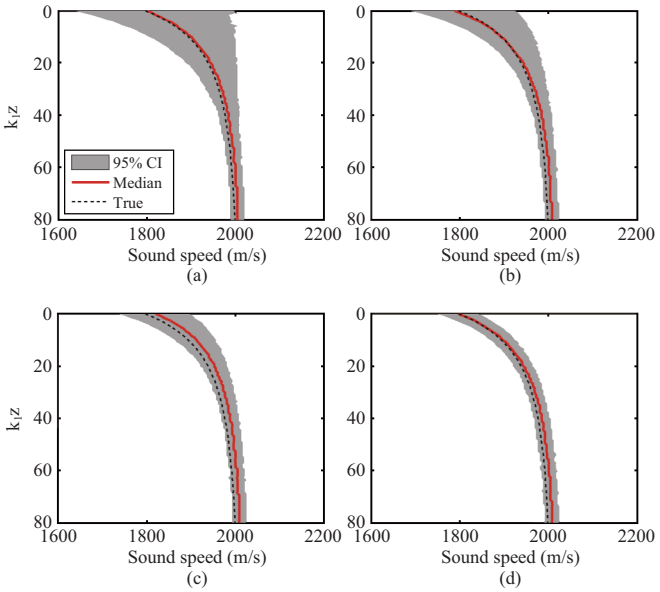

Fig. 7. Effect of SNR on the probability distributions of the reconstructed sediment sound speed profile using the reflection coefficients measured at 75°, 80°, 85° and 90°. (a) uniform distributions of the model parameters, (b) PPD of m inferred from the observed data of SNR = 10 dB, (c) SNR = 20 dB, and (d) SNR = 30 dB.

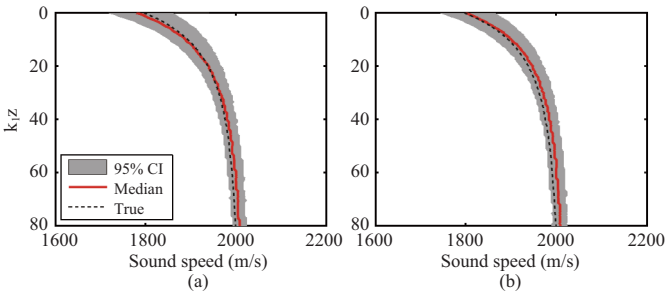

Fig. 8. Effect of the number of measured reflection coefficients on the probability distributions of the reconstructed sediment sound speed profile for SNR = 20 dB at the interval of grazing angle between 75° and 90° with (a) 3° increment (N = 6) and (b) 1° increment (N = 16).

of the environment alone without consultation with the measured data, while for the posterior cases, the inversion in effect extracts additional information from the measurements, and therefore, a better estimation is achieved. It is also noticed that the variation of the prediction near the lower boundary is smaller than that near the upper boundary due to the constraints imposed by the boundary conditions requiring the continuity of sound speed with the seafloor at the lower boundary.

Fig. 8 compares the results inverted from data vectors with different dimensions for SNR = 20 dB. The subplot (a) corresponds to data vector with dimension N = 6, i.e., 6 measurements, while the subplot (b) with dimension N = 16, all equally-sampled from the interval of grazing angles ranging between 75° and 90°. The results illustrate that the prediction is slightly better for N = 16 than that for N = 6, but not much.

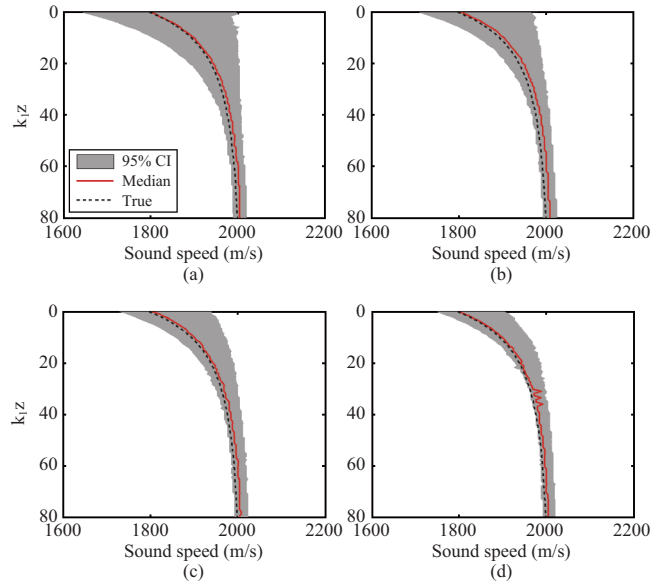

Fig. 9. Effect of SNR on the probability distributions of the reconstructed sediment sound speed profile using the reflection coefficients measured at 45°, 50°, 55° and 60°. (a) uniform distributions of the model parameters, (b) PPD of m inferred from the observed data of SNR = 10 dB, (c) SNR = 20 dB, and (d) SNR = 30 dB.

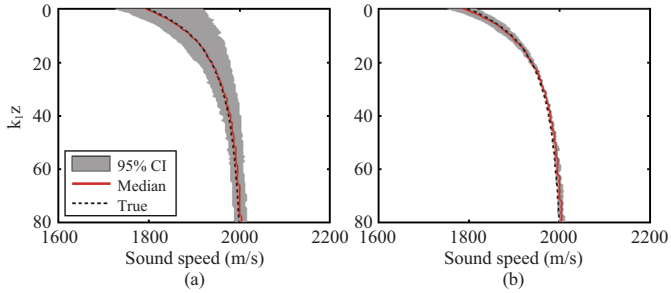

Fig. 10. Effect of the number of measured reflection coefficients on the probability distributions of the reconstructed sediment sound speed profile for SNR = 20 dB at the interval of grazing angle between 45° and 60° with (a) 3° increment (N = 6) and (b) 1° increment (N = 16).

This indicates that the prediction is rather stable when the data are sampled from the region corresponding to steeper grazing angles. These results may also be inferred from the reflection coefficient itself, as shown in Fig. 6(a), in that the reflection coefficients shows less variation in the interval within the range of higher grazing angles.

The results corresponding to Figs. 7 and 8 for lower grazing angles between 45° and 60° are shown in Figs. 9 and 10, respectively. By comparing these figures, it is seen that for the data set sampled from the interval containing highly-oscillatory reflection coefficients (see Fig. 6(a)), the results are in general more uncertain, as evidently shown in comparison of Fig. 7(d) with Fig. 9(d). This is also expected in that for lower grazing angles, the interference due to multiple reflections from various layers in a stratified medium becomes more

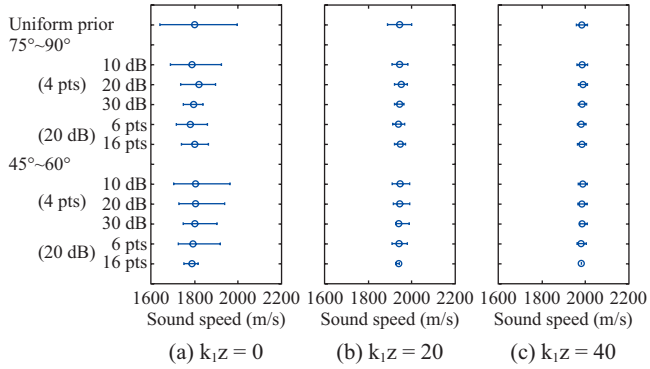

Fig. 11. Comparison of the summary statistics from the various cases studied in Figs. (7)-(10). The circle indicates the median and the error bar indicates 95% CI. The panels from left to right show the summary statistics of the sound speed at different depths in terms of *kz*.

complicated, resulting in a complicated reflection pattern. Under this situation, the uncertainty of the prediction may be compensated by increasing the dimension of the data vector, i.e., the number of data points, as shown in Fig. 10. Here, it shows that by increasing the dimension from N = 6 to N = 16, the uncertainties are greatly reduced, and the results are even better than those inverted from higher angles.

The above results show an interesting interplay between the role of the region in which the data are sampled and that of the number of data measured. For data collected from the region of higher grazing angles, each data set contains more or less alike information so that the results are hardly improved by increasing the number of data points; while for lower grazing angles, the information embedded in the different sets of data has higher degree of diversity, signifying the "amount" of information containing in the lower grazing angles is more than that in the high grazing angles.

The inversion statistics corresponding to three values of sediment depth in terms of k_1z, equal to 0 (at the upper boundary), 20, and 40 (from left to right), are summarized in Fig. 11. These figures present the median and the error bar of the sound speed at three different depths with respect to SNR and data dimension. It is clearly shown that the error bars decrease with increasing depth, as discussed previously due to the constraint of the boundary conditions enforced at the lower boundary of the sediment layer.

VI. CONCLUDING REMARKS

This paper analytically studies the inversion of a sediment sound speed profile using a parameterized geoacoustic model based upon the problem of plane-wave reflection from a non-uniform sediment layer. The inversion gives an estimate of the complete sound speed distribution of the sediment layer, rather than a single value as in the traditional analysis. The primary objective of this paper is to establish the inversion procedure and to analyze the uncertainty with respect to various statistical and/or physical parameters.

The study emphasizes the analysis of estimation uncertainty of the resulted sound speed profiles under various effects. The uncertainty bears significance not only in relation to inversion processes but also to the geoacoustic properties of seabed. Furthermore, one should be also aware of the fact that, in practical applications, the data for reflection coefficients are often measured by a vertical or horizontal array with limited angular resolution, rather than a specific angle as designated in this analysis. As a result, the uncertainty of the estimation is expected to increase due to angular variations of the input reflection coefficients.

While we claim no universal applications of the present study, this analysis provides a basis on the estimation of the geoacoustic properties for a continuously-stratified medium, and is particularly efficient for a medium with properties that can be described by analytical functions.

APPENDIX A: FORMULATION FOR PLANE-WAVE REFLECTION FROM A NON-UNIFORM SEABED

Consider a plane wave of frequency ω, impinging at grazing angle θ upon a flat seabed consisting of a non-uniform fluid-like sediment layer overlying on an elastic basement as schematically shown in Fig. 2. The incident wave lying on x-z plane is represented as $\phi_i(x,z,t) = e^{i[k_x x - k_{z1}(z-h/2)] - i\omega t}$, where $k_x = k_1 \cos\theta$ is the horizontal wavenumber, with $k_1 = \omega/c_1$, $k_{z1} = \sqrt{k_1^2 - k_x^2}$, and c_1 and h being the sound speed of the upper layer and the thickness of the sediment layer, respectively.

Let $\phi_{j,\omega}$ (j = 1 − 3) denote the compressional velocity potential of frequency ω for layer j, and $\psi_{3,\omega}$ the shear velocity potential for layer 3, then the Helmholtz equations describing the 2-dimensional acoustic waves in the various layers are:

$$\left(\nabla^2 + k_1^2\right)\phi_{1,\omega}(x,z) = 0 \tag{A1}$$

$$\left(\nabla^2 + \frac{\omega^2}{c^2(z)}\right)\phi_{2,\omega}(x,z) = \frac{1}{\rho(z)}\nabla\rho(z)\cdot\nabla\phi_{2,\omega} \tag{A2}$$

$$\left(\nabla^2 + k_{3p}^2\right)\phi_{3,\omega}(x,z) = 0 \tag{A3}$$

$$\left(\nabla^2 + k_{3s}^2\right)\psi_{3,\omega}(x,z) = 0 \tag{A4}$$

where $k_{3p} = \omega/c_{3p}$, $k_{3s} = \omega/c_{3s}$ are the compressional and shear wavenumbers of layer 3, and $\phi_{1,\omega}$ is for the reflected field only. It is noted that the density $\rho(z)$ and the sound speed $c(z)$ in Eq. (A2) may vary with respect to depth, and are assumed in the present study to take the form as shown in Eqs. (1) and (2), respectively.

The solutions for Eqs. (A1), (A3), and (A4) are rather straightforward. As for Eq. (A2), it has been solved analytically by Robins [21] to give:

$$\phi_{2,\omega}(x,z) = \left[A_2^-(k_x)G(k_x,z) + A_2^+(k_x)H(k_x,z)\right]e^{ik_x x} \tag{A5}$$

where A_2^+ and A_2^- are unknown constants, and the functions G and H are given by:

$$G(k_x,z) = \sqrt{\zeta(z)}H_\xi^{(1)}(\kappa\zeta(z)) \tag{A6}$$

$$H(k_x,z) = \sqrt{\zeta(z)}H_\xi^{(2)}(\kappa\zeta(z)) \tag{A7}$$

with $H_\xi^{(1)}$ and $H_\xi^{(2)}$ being the ξth-order Hankel functions of the first and second kind, respectively. The relevant variables are defined below:

$$\zeta = 1 - \gamma z \tag{A8}$$

$$\xi^2 = \frac{1}{4} - \frac{\omega^2}{\gamma^2}\left(\frac{1}{c_{2\text{mid}}^2} - \frac{b^2}{c_1^2}\right) \tag{A9}$$

$$\kappa^2 = \frac{1}{\gamma^2}\left(k_1^2 b^2 - k_x^2 - \frac{\beta^2}{4}\right) \tag{A10}$$

Therefore, the solutions corresponding to Eqs. (A1)-(A4) with the x-dependence $e^{ik_x x}$ extracted may be expressed as:

$$\tilde{\phi}_{1,\omega}(k_x,z) = A_1^+(k_x)e^{ik_{z1}(z-\frac{h}{2})} \tag{A11}$$

$$\tilde{\phi}_{2,\omega}(k_x,z) = A_2^-(k_x)G(k_x,z) + A_2^+(k_x)H(k_x,z) \tag{A12}$$

$$\tilde{\phi}_{3,\omega}(k_x,z) = A_3^-(k_x)e^{-\alpha_{3p}(z+\frac{h}{2})} \tag{A13}$$

$$\tilde{\psi}_{3,\omega}(k_x,z) = B_3^-(k_x)e^{-\alpha_{3s}(z+\frac{h}{2})} \tag{A14}$$

where $\alpha_{3p} = \sqrt{k_x^2 - k_{3p}^2}$ and $\alpha_{3s} = \sqrt{k_x^2 - k_{3s}^2}$, and the unknown amplitudes A_1^+, A_2^-, A_2^+, A_3^-, and B_3^- are to be determined from boundary conditions.

For the problem under consideration, the physical boundary conditions are:

$$d_{z,1}\Big|_{z=\frac{h}{2}} = d_{z,2}\Big|_{z=\frac{h}{2}} \tag{A15}$$

$$p_1\Big|_{z=\frac{h}{2}} = p_2\Big|_{z=\frac{h}{2}} \tag{A16}$$

$$d_{z,2}\Big|_{z=-\frac{h}{2}} = d_{z,3}\Big|_{z=-\frac{h}{2}} \tag{A17}$$

$$p_2\Big|_{z=-\frac{h}{2}} = -\sigma_{zz,3}\Big|_{z=-\frac{h}{2}} \tag{A18}$$

$$0 = \sigma_{xz,3}\Big|_{z=-\frac{h}{2}} \tag{A19}$$

where d_z, p, σ_{zz}, and σ_{xz} are vertical displacement, pressure, normal stress, and shear stress, respectively; these variables are related with the velocity potential through its definition and stress-strain relations [15]. After applying these boundary conditions to Eqs. (A11)-(A14), a linear system is produced:

$$\tilde{B}(k_x)\tilde{\chi}(k_x) = \tilde{C}(k_x) \tag{A20}$$

where the coefficient matrix, also referred to as propagator matrix, $\tilde{B}(k_x)$, amplitude vector $\tilde{\chi}(k_x)$, and $\tilde{C}(k_x)$ are given below:

$$\tilde{B}(k_x) = \begin{bmatrix} ik_{z1} & -\frac{\partial G}{\partial z}(k_x,\frac{h}{2}) & -\frac{\partial H}{\partial z}(k_x,\frac{h}{2}) \\ \rho_1 & -\rho_{2\mathrm{U}}G(k_x,\frac{h}{2}) & -\rho_{2\mathrm{U}}H(k_x,\frac{h}{2}) \\ 0 & \frac{\partial G}{\partial z}(k_x,-\frac{h}{2}) & \frac{\partial H}{\partial z}(k_x,-\frac{h}{2}) \\ 0 & \rho_{2\mathrm{L}}\omega^2 G(k_x,-\frac{h}{2}) & \rho_{2\mathrm{L}}\omega^2 H(k_x,-\frac{h}{2}) \\ 0 & 0 & 0 \end{bmatrix}$$

$$\begin{bmatrix} 0 & 0 \\ 0 & 0 \\ \alpha_{3p} & ik_x \\ \lambda_{\mathrm{L}}[(-k_x^2+\alpha_{3p}^2)+2\mu_{\mathrm{L}}\alpha_{3p}^2] & 2i\mu_{\mathrm{L}}k_x\alpha_{3s} \\ -2i\mu_{\mathrm{L}}k_x\alpha_{3p} & \mu_{\mathrm{L}}(k_x^2+\alpha_{3s}^2) \end{bmatrix} \tag{A21}$$

$$\tilde{\chi}(k_x) = \begin{bmatrix} A_1^+(k_x) & A_2^-(k_x) & A_2^+(k_x) & A_3^-(k_x) & B_3^-(k_x) \end{bmatrix}^T \tag{A22}$$

$$\tilde{C}(k_x) = \begin{bmatrix} -ik_{z1} & \rho_1 & 0 & 0 & 0 \end{bmatrix}^T \tag{A23}$$

The parameters $\rho_{2\mathrm{U}}$ and $\rho_{2\mathrm{L}}$ are the density of the layer 2 at the upper and lower boundaries, respectively; also, λ_{L} and μ_{L} are the Lamé constants of the seafloor.

ACKNOWLEDGMENTS

This work was supported in part by National Science Council of Taiwan, R.O.C. through contract NSC 98-2611-M-002-017-MY3, NSC 99-2221-E-110-093, and by the Ministry of Education of Taiwan, R.O.C. under the project entitled Aim for Top University-Asian Pacific Ocean Research Center (95C100303). The authors would like to express our profound thanks for their financial support.

REFERENCES

1. Battle, D., Gerstoft, P., Hodgkiss, W. S., Kuperman, W. A., and Nielsen, P. L., "Bayesian model selection applied to self-noise geoacoustic inversion," *Journal of the Acoustical Society of America*, Vol. 116, pp. 2043-2056 (2004).
2. Box, G. E. P. and Tiao, G. C., *Bayesian Inference in Statistical Analysis*, Addison-Wesley, New York (1992).
3. Dettmer, J., Dosso, S. E., and Holland, C. W., "Joint time/frequency-domain inversion of reflection data for seabed geoacoustic profiles and uncertainties," *Journal of the Acoustical Society of America*, Vol. 123, pp. 1306-1317 (2008).
4. Dosso, S. E. and Holland, C. W., "Geoacoustic uncertainties from viscoelastic inversion of seabed reflection data," *IEEE Journal of Oceanic Engineering*, Vol. 31, pp. 657-671 (2006).
5. Dosso, S. E., Nielsen, P. L., and Wilmut, M. J., "Data error covariance in matched-field geoacoustic inversion," *Journal of the Acoustical Society of America*, Vol. 119, pp. 208-219 (2006).
6. Gerstoft, P., "Inversion of seismoacoustic data using genetic algorithms and *a posteriori* probability distributions," *Journal of the Acoustical Society of America*, Vol. 95, pp. 770-782 (1994).
7. Gerstoft, P., *SAGA Users Guide 5.0, An Inversion Software Package*, An updated version of "SAGA 2.0," SACLANT Undersea Research Centre, SM- 333, La Spezia, Italy (1997).
8. Hamilton, E. L., "Geoacoustic modeling of the seafloor," *Journal of the Acoustical Society of America*, Vol. 68, pp. 1313-1340 (1980).
9. Hamilton, E. L., "Acoustic properties of sediments," in: Lara-Sáenz, A., Ranz-Guerra, C., and Carbó-Fité, C. (Eds.), *Acoustics and Ocean Bottom*, Consejo Superior de Investigaciones Cientificas (CSIC), Madrid, pp. 3-58 (1987).
10. Holland, C. W., "Geoacoustic inversion for fine-grained sediments," *Journal of the Acoustical Society of America*, Vol. 111, pp. 1560-1564 (2002).
11. Holland, C. W., Dettmer, J., and Dosso, S. E.,"Remote sensing of sediment density and velocity gradients in the transition layer," *Journal of the Acoustical Society of America*, Vol. 118, pp. 163-177 (2005).
12. Holland, C. W., Nielsen, P. L., Dettmer, J., and Dosso, S. E., "Resolving mesoscale seabed variability using reflection measurements from an autonomous underwater vehicle," *Journal of the Acoustical Society of America*, Vol. 131, pp. 1066-1078 (2012).
13. Huang, C.-F., Gerstoft, P., and Hodgkiss, W. S., "Uncertainty analysis in matched-field geoacoustic inversions," *Journal of the Acoustical Society of America*, Vol. 119, pp. 197-207 (2006).
14. Huang, C.-F. and Hodgkiss, W. S., "Matched field geoacoustic inversion of low frequency source tow data from the ASIAEX East China Sea experiment," *IEEE Journal of Oceanic Engineering*, Vol. 29, pp. 952-963 (2004).
15. Hudson, J. A., *The Excitation and Propagation of Elastic Waves*, Chapter 1, Cambridge University Press, p. 15 (1987).
16. Jiang, Y.-M., Chapman, N. R., and Badiey, M., "Quantifying the uncertainty of geoacoustic parameter estimates for the New Jersey shelf by inverting air gun data," *Journal of the Acoustical Society of America*, Vol. 121, pp. 1879-1894 (2007).
17. Liu, J.-Y. and Huang, C.-F. "Acoustic plane wave refection from a rough surface over a random fluid half-space," *Ocean Engineering*, Vol. 28, pp. 751-762 (2001).
18. Liu, J.-Y., Huang, C.-F., and Shyue, S. W., "Effects of seabed properties on acoustic wave fields in a seimo-acoustic ocean waveguide," *Ocean Engineering*, Vol. 28, pp. 1437-1459 (2001).
19. Liu, J.-Y., Tsai, S.-H., and Lin, I.-C., "Acoustic wave scattering from a rough seabed over a sediment layer with generalized-exponential density

and inverse-square sound speed profiles," *Ocean Engineering*, Vol. 31, pp. 417-434 (2004).
20. Mosegaard, K. and Sambridge, M., "Monte Carlo analysis of inverse problems," *Inverse Problems*, Vol. 18, pp. 29-54 (2002).
21. Robins, A. J., "Reflection of a plane wave from a fluid layer with continuously varying density and sound speed," *Journal of the Acoustical Society of America*, Vol. 89, pp. 1686-1696 (1991).
22. Schmidt, H., *OASES Version 3.1: User Guide and Reference Manual*, Massachusetts Institute of Technology, Cambridge, MA (1999).
23. Siderius, M., Nielsen, P. L., and Gerstoft, P., "Range-dependent seabed characterization by inversion of acoustic data from a towed receiver array," *Journal of the Acoustical Society of America*, Vol. 112, pp. 1523-1535 (2002).
24. Tarantola, A., Inverse Problem Theory and Methods for Model Parameter Estimation. SIAM, Philadelphia (2005).
25. Tollefsen, D., Dosso, S. E., and Wilmut, M. J., "Matched-field geoacoustic inversion with a horizontal array and low-level source," *Journal of the Acoustical Society of America*, Vol. 120, pp. 221-230 (2006).